



OPEN

Developing Gradient Metal Alloys through Radial Deposition Additive Manufacturing

SUBJECT AREAS:
MATERIALS SCIENCE
ENGINEERINGReceived
4 February 2014Accepted
27 May 2014Published
19 June 2014Correspondence and
requests for materials
should be addressed to
D.C.H. (dch@jpl.nasa.
gov)Douglas C. Hofmann^{1,2}, Scott Roberts^{1,2}, Richard Otis^{1,3}, Joanna Kolodziejaska^{1,2}, R. Peter Dillon¹, Jong-ook Suh¹, Andrew A. Shapiro^{1,2}, Zi-Kui Liu³ & John-Paul Borgonia¹¹Engineering and Science Directorate, Jet Propulsion Laboratory, California Institute of Technology, 4800 Oak Grove Dr. Pasadena CA 91109, ²Keck Laboratory of Engineering Sciences, California Institute of Technology, 1200 E. California Blvd., Pasadena CA 91125, ³Department of Materials Science and Engineering, Pennsylvania State University, University Park PA 16802.

Interest in additive manufacturing (AM) has dramatically expanded in the last several years, owing to the paradigm shift that the process provides over conventional manufacturing. Although the vast majority of recent work in AM has focused on three-dimensional printing in polymers, AM techniques for fabricating metal alloys have been available for more than a decade. Here, laser deposition (LD) is used to fabricate multifunctional metal alloys that have a strategically graded composition to alter their mechanical and physical properties. Using the technique in combination with rotational deposition enables fabrication of compositional gradients radially from the center of a sample. A roadmap for developing gradient alloys is presented that uses multi-component phase diagrams as maps for composition selection so as to avoid unwanted phases. Practical applications for the new technology are demonstrated in low-coefficient of thermal expansion radially graded metal inserts for carbon-fiber spacecraft panels.

Additive Manufacturing (AM), also known as three-dimensional printing or layer manufacturing, is a freeform fabrication process by which an object is built up, layer by layer, via selective deposition of material¹. In contrast to conventional computer-controlled machining, where a tool path is created to remove material from a billet dimensionally larger than the final part, AM uses a tool path which slices the desired part into discrete two-dimensional layers which are then deposited consecutively to additively build the part. The AM process is unique compared with other manufacturing technologies because a piece of hardware can be built in freeform, without the removal of material and without the creation of a mold^{2,3}. This has many benefits, including the ability to do rapid prototyping and the fabrication of parts with blind machining features. Using AM with plastics has been well established over the last decade and equipment is available at all scales, from tabletop printers to industrial machines capable of producing proof of concept mock-ups and actual consumer products. Thermoplastic polymers are generally ideal materials for AM, owing to the fact that they have low melting temperatures and high viscosities which allows for simple resistance heaters and nozzles to be used for precise deposition. Polymer AM is low cost and widely accessible technique for fabricating three-dimensional objects.

The benefits of freeform three-dimensional printing also extend to metal alloys, although, unlike polymers, the higher melting temperatures of structural metals limit the available heating methods and the viscosity of molten metal is much lower than thermoplastic polymers so continuous feeding is difficult (for example, injection molding of polymers is done at viscosities of $\sim 10^3$ Pa·s while molten metals have viscosities of $\sim 10^{-3}$ Pa·s). The AM techniques that have been shown to be successful for metals include rastering metal powder with a laser, ultrasonically welding metal tape, introducing metal wire into an electron beam and introducing metal powder into a laser beam⁴. Two of the most mature technologies for AM with metals are direct metal laser sintering (DMLS) and Laser Deposition (LD), both of which use the consolidation of a powder with a laser heating source. In DMLS a computer-controlled laser is rastered across a bed of metal powder, consolidating only the powder that was subjected to the laser heating⁵. After each layer has been consolidated, the workbench lowers and a new layer of powder is brushed over the workpiece and the consolidation is repeated. Once the part is completed, it is removed from the loose powder and may subsequently be heat-treated or finish-machined to remove the rough outer surface layer. LD works by introducing the metal powder directly into the laser beam as the build head rasters over the work piece. The laser creates a liquid melt pool as it rasters, allowing for a fully dense part to be



built up, layer-by-layer, with well-densified bonds between layers⁶. Both DMLS and LD are being widely evaluated as alternative methods for fabricating metal components with versions of the machines in industry, academia and national laboratories.

Since the development of AM in metals, much of the research and technology development has focused on reducing manufacturing costs (relative to conventional machining), fabricating parts that cannot be easily machined using other techniques, and qualifying parts fabricated by AM to verify compliance with existing material standards. One of the most beneficial applications of AM with metals, however, is the ability to create net-shaped parts with custom compositions. The LD process is ideally suited to create these alloys, owing to the ease by which different elemental or alloy powders can be introduced into the melt pool during the fabrication process. Functionally graded materials, of which gradient metal alloys are one category, were theorized in the early 70 s and have been investigated for some time, yet following national research programs in both Japan and Germany these materials have found only limited commercial use^{7–9}. Advances in additive manufacturing, particularly in laser deposition, are increasingly suitable for mainstream production of functionally graded materials and metal alloys. Herein, a methodology for creating gradient alloys is provided, which includes the concept of using multi-component phase diagrams as maps for gradient composition selection, the development of several prototype gradient alloys with multifunctional properties, and the demonstration of the benefits of the technique through a prototype application. In this work, the gradient AM process is utilized to fabricate near net-shaped parts where composition can be controlled strategically through the part in a linear or radial method. This demonstrates that hardware can be fabricated with multifunctionality that is difficult to achieve using other manufacturing methods.

There has been extensive work correlating LD process parameters such as scan speed and laser power to the temporal and spatial temperature profile of the system¹⁰. Determination of this profile is key to making accurate predictions of the microstructural evolution and, ultimately, the mechanical properties of the finished piece. This is especially important for two-phase titanium alloys (e.g. Ti-6Al-4V) as the α/β microstructures are highly sensitive to thermo-mechanical processing¹¹. There have been several studies on microstructural evolution in LD titanium alloys^{12–14}, including several on the effects of compositional grading with β -stabilizers on microstructure^{15–17}. For all of the work that has been done characterizing the microstructural evolution and mechanical behavior of gradient alloys, relatively little attention has been paid to how they might be designed using a systematic approach. A common problem in compositional grading is the formation of brittle phases which often have a detrimental effect on mechanical properties. A new approach, outlined in detail in this work, is to use alloying elements to thermodynamically stabilize desirable phases, effectively side-stepping problematic areas of alloy composition space. Knowledge of metastable and stable phase equilibria in the multi-component alloy system and how these equilibria influence the microstructure under given processing conditions allow for rapid determination of whether a particular gradient is sufficiently feasible to warrant an experimental investigation.

In the current work, gradient alloys were fabricated using a four-hopper RPM 557 Laser Deposition System (LDS) with YAG laser and inert atmosphere at RPM and Associates Inc., South Dakota. Similar to laser-engineered net shaping (LENS[®]) which uses a CO₂ or YAG laser, a molten metal pool is sustained as metal powder is deposited. The system allows for the addition of up to four separate elemental or alloy powders during fabrication where the volume fraction of powder can be changed by ~1% per deposited layer. New alloy combinations were fabricated into a number of geometries and both alloy and elemental powders were used during fabrication. The laser power was continuously optimized (between 200–900 W), the volume fraction of mixed powders was varied

in steps ranging from 1–100%, and the thickness of the deposited layers ranged from 0.25–0.50 mm.

To illustrate the fabrication of a gradient alloy, Fig. 1 shows a test sample that was fabricated via LD using a rule-of-mixtures of Ti-6Al-4V (Ti_{86.2}Al_{10.2}V_{3.6} in at.%) powder and elemental vanadium (V) powder. The gradient was produced by depositing the Ti-6Al-4V powder directly onto a 6.35 mm thick Ti-6Al-4V plate before adding V in 3% volume increments until the part fully transitioned to V. The power was held constant at 600 W and deposition of 195 individual 0.38 mm thick layers occurred in 585 min under 4.4 lpm of Ar. For each of the 35 individual compositions comprising the gradient between Ti-6Al-4V and V, between 4 to 5 layers were deposited to assure a sufficiently thick region for mechanical testing, microscopy and x-ray diffraction. The run log for the fabrication is shown in Table 1. It should be noted that while the deposition process was repeatable and produced fully dense parts, there exist a number of process variables that can be optimized. Among the parameters that can be adjusted and/or optimized during the deposition process are the thickness of the layers, the dwell time before the fabrication of the next layer, the step size of the gradient, the thickness of the substrate (which affects cooling), the laser power (which is related to temperature through the reflectivity of the powder), the atmosphere (typically Ar), the rate of powder feed, the laser travel speed, the tilt angle, the working height, the spot size of the laser, the velocity of part rotation (for radial parts), and the purity of the powder feedstock.

Fig. 1a shows a schematic model of the building head used in the LD process. The location of the 4 nozzles which draw metal powder from hoppers and introduce it into the laser is shown in Fig. 1b. A hollow cylinder, a rectangular beam and a square beam are shown being fabricated in Fig. 1c. A representative “forest” of test specimen posts is shown in Fig. 1d, which were used to vary building parameters. SEM of the gradient cross-section revealed no porosity, indicating that the laser power was sufficient to create a molten pool during deposition. Fig. 1e shows the average hardness (Rockwell C) of the Ti-6Al-4V to V gradient alloy across the compositionally graded sample. X-ray diffraction patterns from selected regions are shown in the inset (i–v). Hexagonal closed packed (HCP), or α phase, Ti-6Al-4V was initially deposited with a nominal hardness for the annealed wrought alloy similar to that typically observed in AM Ti-alloys produced by similar methods. At approximately 10.5 mm from the baseplate, V is introduced to the Ti-6Al-4V resulting in a hardening of the HCP titanium alloy. With increasing V, the alloy transformed to a softer phase which continued to soften during the transition to pure V.

X-ray diffraction across the gradient (Fig. 1e) shows the stabilization of the softer body centered cubic (BCC) β -phase of titanium as vanadium content increases. With increasing V, the hardness is relatively level near 30 Rockwell C until the sample is >90% V, at which point the hardness drops to the value of pure annealed V, approximately 1–2 Rockwell C. The volume of a unit cell for each x-ray scan was calculated and is shown at the right of Fig. 1e. HCP and BCC coexist in the alloy and the volume of the unit cell decreases linearly by 6 Å³ from the transition to BCC until the alloy is pure V. A three-dimension map, Fig. 1f, was compiled from x-ray scans of the gradient alloy sliced into 1 mm thick pieces and scanned on each side. The map shows the HCP Ti side of the gradient, a region where HCP and BCC coexist, and a BCC region with decreasing lattice parameter (observed by the shift in the lattice peaks) as the V content increased.

The Ti-6Al-4V to V gradient is very illustrative of the process by which metals can be functionally graded. Ti-6Al-4V and V have different equilibrium crystal structures (HCP vs. BCC), yield strengths (828 MPa vs. 776 MPa), hardness (46 vs. 2 Rockwell C), densities (4.42 vs. 6.11 g/cm³), and melting temperature (1947 K vs. 2008 K) among others; however, what makes the gradient possible is the lack of brittle phases at all of the intermediate compositions. Consider that the effect of diffusion on a deposited composition

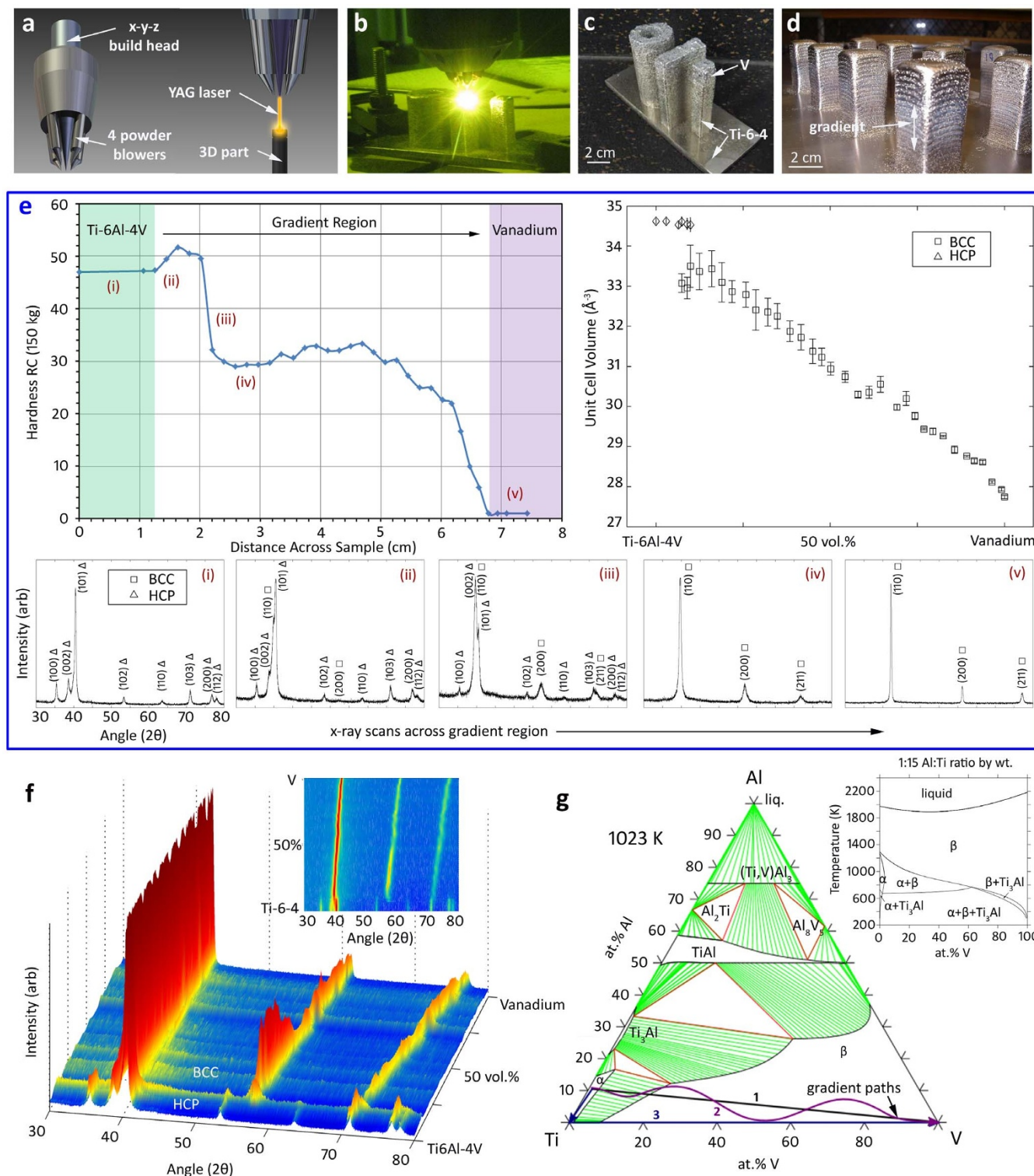


Figure 1 | Analyzing a Ti-6Al-4V to V Gradient Alloy. – (a) Schematic of the laser deposition (LD) building heads used to fabricate gradient alloys. (b) Image of the LD process fabricating several test specimens of the Ti-V gradients. (c) Three gradient alloy specimens; a hollow cylinder, a plate and a beam. (d) Example of a “forest” of gradient alloy posts used to vary gradient compositions. (e) A plot of Rockwell C hardness vs. distance across at Ti-6Al-4V to V gradient alloy where x-ray scans from locations (i–v) are shown below the figure. At right is a plot showing unit cell volume throughout the gradient, as measured from the x-ray peaks. (f) A 3D map of x-ray peaks across the gradient alloy showing the transition from HCP to BCC and the lattice shift of BCC (2D shown in the inset). (g) A Ti-Al-V vertical section at 1023 K. Path (1) is the rule-of-mixtures between Ti-6Al-4V powder and V powder. Path (2) represents a gradient path which transitions from Ti-6Al-4V to pure Ti then to pure V. Path (3) is meant to illustrate a freeform path, where the composition can be changed continuously by mixing Ti, Al and V elemental powder.

can be neglected as long as the residence time of the laser is much shorter than the characteristic time for bulk transport of solid particles in the melt pool (Mortensen and Suresh, *Int. Mater. Rev.*, 1995),

and steep thermal gradients induced by the laser ensure that solid-state mass transport quickly becomes kinetically negligible. Every point along the composition gradient can then be treated as locally



Table 1 | Fabricating a Ti-6Al-4V to V Gradient Alloy – Run log showing the manufacture of a gradient alloy using a blend of 325 mesh Ti-6Al-4V powder and pure V powder. The building power was 600 W, each layer is 0.38 mm thick and the total build time was 585 minutes

Layers	% vol Ti-6Al-4V	% vol V	g/min Ti-6Al-4V	g/min V
0–28	100%	0%	2.10	0.00
29–33	97%	3%	2.04	0.08
34–38	94%	6%	1.97	0.16
39–43	91%	9%	1.91	0.24
44–48	88%	12%	1.85	0.31
49–53	85%	15%	1.79	0.39
54–58	82%	18%	1.72	0.47
59–63	79%	21%	1.66	0.55
64–68	76%	24%	1.59	0.63
69–73	73%	27%	1.53	0.71
74–78	70%	30%	1.47	0.78
79–83	67%	33%	1.41	0.86
84–88	64%	36%	1.34	0.91
89–93	61%	39%	1.28	1.02
94–98	58%	42%	1.22	1.10
99–103	55%	45%	1.16	1.18
104–108	52%	48%	1.09	1.26
109–113	49%	51%	1.57	2.03
114–118	46%	54%	1.52	2.15
119–123	43%	57%	1.42	2.27
124–128	40%	60%	1.32	2.39
129–133	37%	63%	1.22	2.51
134–138	34%	66%	1.12	2.63
139–143	31%	69%	1.02	2.75
144–148	28%	72%	0.92	2.87
149–153	25%	75%	0.83	2.99
154–158	22%	78%	0.73	3.11
159–162	19%	81%	0.62	3.23
163–166	16%	84%	0.53	3.35
167–170	13%	87%	0.43	3.47
171–174	10%	90%	0.30	3.58
175–178	7%	93%	0.23	3.71
179–182	4%	96%	0.13	3.83
183–186	1%	99%	0.03	3.94
187–195	0%	100%	0.00	3.98

at equilibrium. Assuming that the nominal alloy composition is close to the solidified composition (equivalent to neglecting partitioning effects) then the evolution of the composition gradient can be represented by a phase diagram. Examine the continuous-cooling transformation (CCT) diagram for Ti-6Al-4V and note that, for example, the transformation finish temperature, T_f , for Ti-6Al-4V is close to 1023 K (750°C) for the expected cooling rates (J. Sieniawski et al., “Microstructure and Mechanical Properties of High Strength Two-Phase Titanium Alloys,” *InTech*, p. 72, 2013). Assuming T_f is a weak function of composition and fast kinetics above T_f , the final phase composition will closely follow the isothermal section at T_f . This can be illustrated by looking at an isothermal ternary phase diagram at 1023 K for Ti-Al-V, shown in Fig. 1g. The black arrow, denoted “1”, indicates the starting composition at Ti-6Al-4V and terminates in the end composition of V, where the intermediate compositions fall along the line, depending on the step-resolution of the building process. While the actual build is a highly non-isothermal process, the transformation kinetics of the $\beta/(\alpha + \beta)$ reaction are very slow at this temperature, so the room temperature phase fields will appear similar to the equilibrium phase fields near 1023 K under typical LD processing conditions. This is consistent with a phase analysis of the gradient performed by x-ray diffraction. The phase diagram illustrates that with large Al concentrations, there are many ordered compounds that could form (e.g., V_5Al_8 and $TiAl_3$). The gradient from Ti-6Al-4V to V, however, represents a linearly decreasing Al

content from 10 to 0 at. %, avoiding regions where those phases would form.

The selection of a Ti-6Al-4V to V gradient is advantageous because many compositional paths may be followed which are free of brittle, ordered phases (see the constant Ti:Al ratio vertical section in the inset Fig. 1g). This section is very similar to the binary Ti-V phase diagram except that the α -phase field is stabilized by the addition of Al. Not all gradients are as straightforward to fabricate as simply creating a rule of mixtures between two metals or alloys. In most cases, careful attention must be paid to the chemical composition of the “gradient path” to avoid the formation of brittle phases that crack during the building process (although not shown, many trial gradient alloys cracked during fabrication, see the supplementary material).

One advantage of using gradient AM techniques is the ability to fabricate custom compositions, using binary, ternary or quaternary phase diagrams as a map between desired compositions. In contrast to traditional alloy development, where multi-component alloys are made one point at a time until a region of a phase diagram is understood, the gradient process allows for many compositions along a line to be fabricated in the same part. This is desirable for alloy development, because nanoindentation experiments can be used to characterize many compositions in a single sample (Fig. 2) without having to make them individually. It is also desirable for transitioning from one alloy to another to exploit the mechanical or physical properties at each end of the gradient (such as thermal expansion, magnetism or melting temperature, or other material characteristics).

For each gradient alloy, there must be a defined gradient path in composition space selected for the AM building process. There may be many of these paths that could be selected depending on the functionality required by part, see the arrows labeled in Fig. 1g. The path could be linear (representing the most direct route from one composition to another), curved (to avoid unwanted phases), or discontinuous (to create a step in compositions). Because many industrially relevant alloy systems, e.g., Ni-base superalloys, can consist of ten or more components, a systematized approach is needed that enables calculation of multi-component phase diagrams. The CALPHAD method (from “CALculation of PHase Diagrams”) is based on the idea that, once the energy of each phase in a system is known as a function of temperature, composition and/or other thermodynamic variables of interest, phase equilibria can be quantitatively predicted for a given set of conditions, and arbitrary phase diagrams can be constructed¹⁸. For crystalline phases the model form is a compound energy formalism where the total energy is described by the partial occupation of sublattices. At equilibrium, components will partially occupy each sublattice in a way that minimizes the overall energy while satisfying the specified conditions.

$$G_{mf}^{phase}(T, P, N_i) = \Delta_f G_{mf} + \Delta^{id} G_{mf}^{mix} + \Delta^{xs} G_{mf} \quad (1)$$

Equation (1) shows the typical form of a phase model. The Gibbs energy per mole of formula of a phase, G_{mf}^{phase} , is the sum of (a) the Gibbs energy of formation compared to a defined reference state, $\Delta_f G_{mf}$, (b) an ideal mixing contribution, $\Delta^{id} G_{mf}^{mix}$, and (c) an excess contribution that captures all non-ideal interactions, $\Delta^{xs} G_{mf}$. $\Delta_f G_{mf}$ is calculated by summing the energetic contributions from each sublattice component. $\Delta^{xs} G_{mf}$ is calculated from an excess energy model where fitting parameters describe the higher-order composition-, temperature- and pressure-dependence of the energy. In practice these model parameters are tabulated in commercial and public thermodynamic databases used by commercial software packages such as Thermo-Calc¹⁹ or PANDAT²⁰. For well-assessed systems the user needs only to specify the components in the system and the desired sets of conditions to calculate the phase diagram. An advantage of the CALPHAD approach is that the phase diagrams

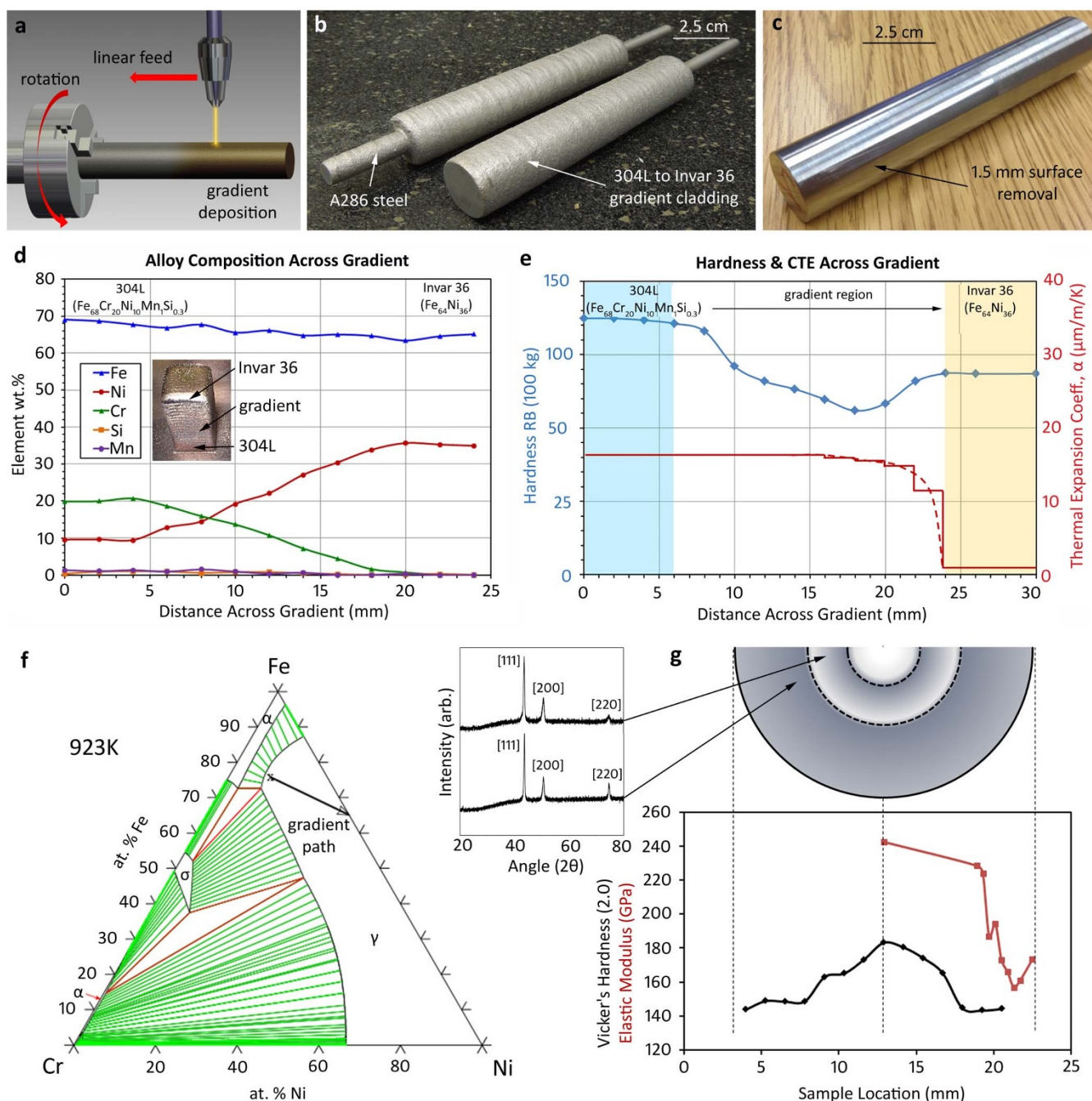


Figure 2 | Developing a radially graded alloy. – (a) Schematic of the rotational deposition process used to develop alloys with gradient compositions in a radial direction. (b) Image of two radially graded alloys where a 304 L to Invar 36 gradient was applied to a rotating A286 stainless steel rod. (c) After removal of 1.5 mm of surface layer, a fully dense gradient rod is obtained. (d) A plot of composition vs. distance for a 304 L to Invar 36 gradient alloy post. (e) A plot of Rockwell B hardness and coefficient of thermal expansion vs. distance for the gradient alloy from (d). Solid red lines connect experimental measurements and dashed lines are theoretical estimates. (f) A calculated phase diagram at 923 K showing a “gradient path” from 304 L to Invar 36. (g) Nanoindentation on the gradient rod shown in (b–c) showing Vickers hardness and modulus (utilizing the same axis). X-ray scans are shown in the insets for two locations near the gradient.

calculated from the models are self-consistent and can be compared to experimental thermochemical data (e.g., calorimetry) as well as phase equilibria data. Because of the relative rarity of quaternary compounds in nature, models of ternary systems can readily be combined to produce models of higher-order systems that may be otherwise infeasible to thoroughly investigate experimentally. Information about the multi-component phase equilibria can be applied to the design of gradient paths that optimize the desired function of the graded part, whether it's a high fracture toughness

transition from one material to another or gradient of mechanical or physical properties.

In a more practical consideration, a gradient alloy may be designed based on limitations in equipment or in metal powder supply. For example, the alloys developed in the current study were fabricated on an LD system with a 4-hopper powder feeder. As is common with most LD equipment, up to four different powders (either alloy or elemental) can be used during gradient builds. To illustrate this, a Ti-6Al-4V part fabricated using this type of equipment could be built



Table 2 | Radial Gradient Building Parameters – Run logs for the 16 layers used to fabricate the radial 304 L to Invar 36 gradient. Listed in the table are the volume % of each powder deposited in that layer, the grams per minute (GPM) deposited, the linear travel speed, the laser power, the rod diameter at the end of the layer, and the rotational velocity of the rod

Layer	% vol 304 L	% vol Invar 36	g/min 304 L	g/min Invar 36	Travel speed (mm/s)	Laser Power (W)	Rod Diameter (mm)	Rotational Velocity (rpm)
0	87.5%	12.5%	6.44	0.93	4.23	290	6.35	12.73
1	75.0%	25.0%	5.52	1.85	4.23	290	6.86	11.79
2	62.5%	37.5%	4.60	2.78	4.23	290	7.37	10.98
3	50.0%	50.0%	3.68	3.70	4.23	290	7.87	10.27
4	37.5%	62.5%	2.08	4.63	4.23	320	8.38	9.65
5	25.0%	75.0%	1.61	5.56	4.23	320	8.89	9.10
6	12.0%	88.0%	1.15	6.48	4.23	320	9.40	8.60
7	0.0%	100.0%	0.69	11.11	6.35	600	9.91	12.24
8	0.0%	100.0%	0.00	11.11	6.35	600	10.92	11.10
9	0.0%	100.0%	0.00	11.11	6.35	600	11.94	10.16
10	0.0%	100.0%	0.00	11.11	6.35	600	12.95	9.36
11	0.0%	100.0%	0.00	11.11	8.47	700	13.97	11.58
12	0.0%	100.0%	0.00	11.11	8.47	700	14.99	10.79
13	0.0%	100.0%	0.00	11.11	8.47	700	16.00	10.11
14	0.0%	100.0%	0.00	11.11	10.58	775	17.02	11.88
15	0.0%	100.0%	0.00	11.11	10.58	775	18.03	11.21
16	0.0%	100.0%	0.00	11.11	10.58	775	19.05	10.61

using a blend of elemental Ti, Al and V powder or by using a powder of the alloy. In many cases, using an alloy powder is preferred to assure the desired composition while minimizing impurities in the final part, particularly for alloys with minor additives (e.g. Mn and Si in 304 stainless steel, Fig. 2). Forming gradient alloys using a rule-of-mixtures of alloy powder is typically more cost effective and more precise at obtaining particular compositions but may limit the gradient paths available. Alternatively, using elemental powder allows for greater control of the major constituent elements to avoid unwanted phases²¹. Fig. 1g demonstrates three arbitrary gradient paths (labeled 1–3) that are possible in the transition from Ti-6Al-4V to elemental V using a Ti-Al-V isotherm at 1023 K and a constant Ti:Al ratio vertical section calculated using the COST 507 database²². Path (1) is simply the rule-of-mixtures between Ti-6Al-4V powder and V powder that was used to fabricate the gradient alloy in Fig. 1. The corresponding vertical section is shown in Fig. 1g. The number of individual compositions in the final gradient is a function of the step size, which represents the change in volume percentage of each alloy powder during the build and the height of each layer. In the current work, the step size is changed from 1–50% to investigate the effect of the gradient fidelity on properties. Path (2) in Fig. 1g represents a gradient path which transitions from Ti-6Al-4V to pure Ti then to pure V. Once the Ti-6Al-4V is transitioned to pure Ti, then the gradient between Ti to V can simply be illustrated with a binary phase diagram. Path (3) is meant to illustrate a freeform path, where the composition can be changed continuously by mixing Ti, Al and V elemental powder. These types of gradients are excellent for avoiding unwanted phases. For instance, the phase diagram shows that formation of a brittle intermetallic phase becomes thermodynamically favorable at higher Al concentrations. In all three gradient paths illustrated in Fig. 1g, Al concentrations above 12 at.% are avoided.

Utilizing the gradient path technique as a design principle, several successful gradient alloys were fabricated (along with many that were unsuccessful). Among these were gradients between Ti-6Al-4V to V, Ti-6Al-4V to Nb, Ti-6Al-4V to V to 420 stainless steel, 304 L stainless steel to Invar 36, 316 L stainless steel to Invar 36, A286 stainless steel to Invar 36, and 304 L stainless steel to Inconel 625. More details about these compositions are shown in the supplementary material.

In Fig. 1, we demonstrated functionally graded metal alloys fabricated orthogonally on the z, or vertical, axis using LD, a well-known AM technique. To increase the utility of the AM process for gradient alloys, we incorporated a rotational axis into the manufacturing

process, illustrated by schematic in Fig. 2a. Unlike previously demonstrated LD processing of monolithic and clad cylindrical forms built up from a flat plate^{23,24}, a metal-precursor rod was rotated via a small motor placed inside the building envelope of the LD system and a gradient alloy was deposited *radially* from the centerline outwards. The build proceeded by first depositing one rotation worth of material, at which point the laser was translated one step linearly along the rod and another rotation was deposited. Once a single layer was deposited along the length of the rod, the composition was changed for the next layer and the process was repeated. An A-286 stainless steel rod (~Fe₅₆Cr₁₅Ni₂₅Mn₂Si₁Ti₁ in wt.%) was selected as the precursor and 304 L stainless steel (~Fe₆₈Cr₂₀Ni₁₀Mn₁Si_{0.3} in wt.%) (which is readily accessible in powder) was deposited on the rod using a combination of linear and rotational motion, (see Table 2 for details). The 304 L was graded to Invar 36 (Fe₆₄Ni₃₆ in wt.%) in steps of 12.5% over a radius of approximately 12 mm, where each layer was approximately 0.5 mm thick. The final gradient rods after fabrication are shown in Fig. 2b, with the A286 rod that was gripped by the motor protruding from the center. Approximately 1.5 mm was removed from the surface using a lathe to achieve the final rod shown in Fig. 2c. Although not shown, the rod was sectioned and viewed using SEM to assure that no porosity or unwanted phases were produced during the fabrication. The radially graded rod was produced to exploit the difference in thermal expansion between stainless steel and Invar 36. To illustrate this, a linear gradient alloy was fabricated between 304 L and Invar 36, shown in Fig. 2d–e, with a smaller 3% volume change per step. The composition across the gradient alloy was measured via energy dispersive x-ray spectroscopy (EDS), shown in Fig. 2d. Both alloys contain a similar wt.% of Fe, which stays relatively constant across the gradient. The Cr in the 304 L is linearly graded to 0% while the Ni is increased from 10% to 36%. The trace elements, among them Si and Mn, are graded away, leaving the binary Invar 36 after 20 mm into the gradient.

Unlike the Ti-6Al-4V to V gradient alloy, which exhibited distinct changes in crystal structure, hardness, and composition, the 304 L to Invar 36 gradient alloy doesn't represent a large change in composition (similar concentrations of Fe exist in both). Instead, this alloy was selected for its dramatic change in coefficient of thermal expansion (CTE), see Fig. 2e. Invar 36 is well-known for having a near-zero CTE at low temperatures and is commonly used in spacecraft optics to match the CTE of silica glass optics. 304 L stainless steel, in contrast, has a CTE of ~17 $\mu\text{m}/\text{m}/\text{K}$, similar to other steels. The gradient

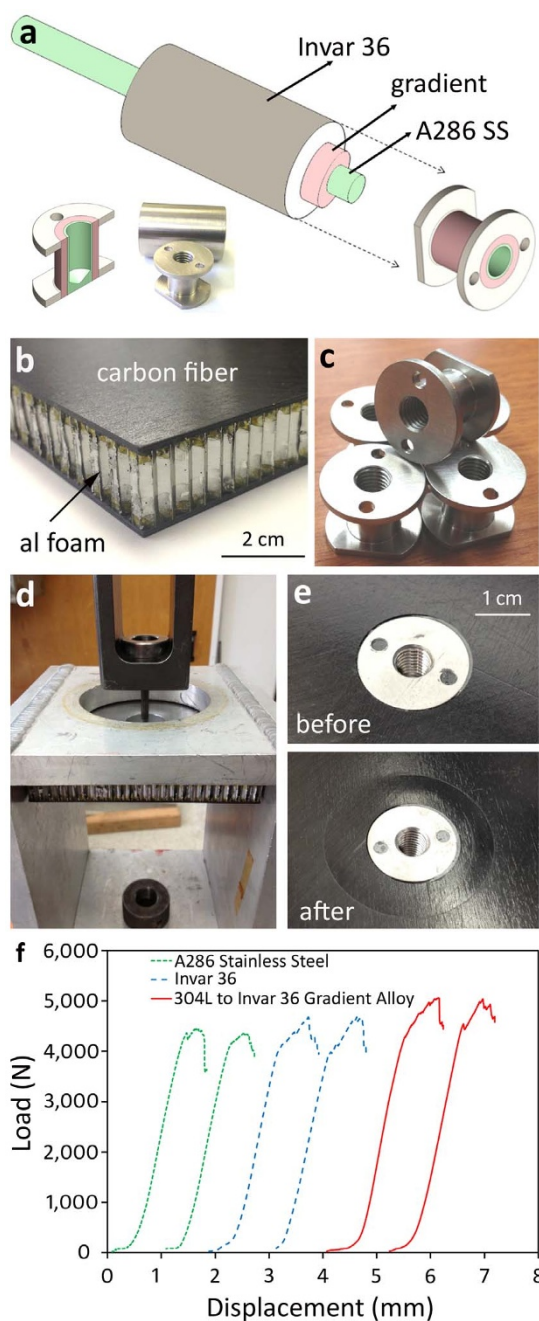


Figure 3 | Gradient Alloys for Carbon Fiber Composite Inserts. – (a) Schematic of how gradient inserts were machined from a radially graded rod, shown in Fig. 2. (b) Enlargement of a carbon fiber/aluminum honeycomb commonly used in spacecraft applications. (c) Examples of identical inserts machined from the gradient alloy, pure Invar and pure A286 steel. (d) Pull-out testing for the low-temperature cycled inserts that have been attached to the panel using epoxy. (e) Before and after images of the insert pull-out tests, showing deformation in the carbon fiber panel. (f) Load vs. displacement curves for the pull-out tests showing that the gradient insert outperformed the monolithic metal ones.

alloy, with composition shown in Fig. 2d, was designed using a Fe-Cr-Ni ternary isothermal phase diagram (where trace elements of Si and Mn were excluded). The thermodynamic database used was a 2011 National Institute of Materials Science (NIMS) assessment based on modeling by Miettinen²⁵. The ternary isotherm at 923 K, shown in Fig. 2f, suggests that a rule-of-mixtures between 304 L and Invar 36 should result in the formation of austenite at intermediate

compositions, assuming that the transformation kinetics below the γ transition temperature are slow. Hardness measurements, shown in Fig. 2e, suggest retention of austenite across the gradient at room temperature. Two selected x-ray diffraction scans, shown in the inset of Fig. 2g, confirmed a single-phase microstructure at all compositions and each intermediate composition was verified to be free from brittle intermetallic phases. The linear gradient alloy was sectioned and the CTE measured using a thermomechanical analyzer (TMA), shown in Fig. 2g for 300–373 K. Since each sample represented a slice of the gradient, a “stepped” plot was obtained to illustrate that the CTE was a rule-of-mixtures average of the entire section. The dotted line represents the average CTE of the gradient alloy. As expected, the Invar 36 side of the gradient exhibited a near-zero CTE, which transitions rapidly back to the value of 304 L stainless steel after a small change in composition. It should be noted that the 304 L to Invar 36 gradient also demonstrated a gradient in ferromagnetism. The Invar side of the gradient was highly magnetic, while the high Cr-content of the 304 L makes it non-magnetic. This observation is the subject of future work.

The 304 L to Invar 36 transition used in the radial gradient alloy, shown in Fig. 2g, exhibits similar mechanical properties to the linear sample. Nanoindentation was used to measure the hardness and the modulus across the radial alloy while x-ray, measured on cut sections of the gradient, exhibits only FCC austenite. In both the linear and radial gradient alloys, the hardness and modulus is larger in the stainless steel than in the Invar 36 but the intermediate compositions are not simple averages of the two. Many new compositions were formed in the gradient region but, as the phase diagrams predict, they were all phases which are known to be soft. Although not shown here, many gradient paths were attempted during experimentation to verify the strategy of mapping the gradient path. Alloys were deliberately steered towards predicted intermetallic phases and, consistently, the samples cracked when encountering these brittle phases.

As Fig. 3 demonstrates, the radial gradient from A286 to 304 L to Invar 36 was designed to exploit the grading of CTE. To illustrate one potential application where radially graded alloys exhibit a benefit in mechanical properties that a wrought alloy does not, consider a carbon fiber insert for use in low-temperature spacecraft panels. Carbon fiber/aluminum foam composites are widely used in spacecraft structures due to their high strength and stiffness, coupled with low density. To attach the panels together or onto other structures, however, metal inserts must be epoxied into holes drilled in the panels. The inserts then provide a threaded hole through which other components can be bolted to the panel. Unfortunately, these panels are often used in low temperatures or experience extreme temperature variation. The CTE mismatch between the low-CTE carbon fiber and the high-CTE metal inserts stresses the epoxy and a phenomenon known as “pullout” occurs. The radial gradient, shown in Fig. 3a, was designed so that the core of the alloy was constructed of A286 stainless steel, the same as the bolts used on some spacecraft. The exterior of the rod, which was graded to Invar 36, exhibits a similarly low-CTE to the carbon fiber panel. 304 L stainless steel was deposited directly onto the A286 bolt in a step-function gradient. Fig. 3a is a schematic showing where the gradient inserts were machined from the gradient rods. Fig. 3b shows tests panels that were fabricated from 8 plies of M55J carbon fiber bonded with resin to Al-5056 honeycomb to form a sandwich panel. The inserts were bonded to the panels using an EA 9394 adhesive, a high modulus adhesive which is known to experience pullout. As control samples, inserts made from wrought A286 and from Invar 36 are shown in Fig. 3b, which were machined identically as the gradient alloy. After bonding, the panels were all subjected to low-temperature thermal cycling from 123–373 K five times for each sample and tension pull-out tests were performed until failure on the A286, Invar 36 and the gradient inserts, shown in Fig. 3d–f. The load vs. displacement curves for two tests performed with each insert type are shown in Fig. 3f. The



gradient inserts were able to support 5000 N of tensile load while the control samples did not exceed 4500 N. The pullout load was therefore higher (~11%) for the radially graded alloy than for the monolithic metal inserts, demonstrating one possible benefit of radially graded alloys.

To conclude, the current work extends upon the literature in gradient alloys by demonstrating a roadmap for producing materials with multifunctional properties that generally cannot be obtained using standard metallurgy techniques. Deposition experimentation was combined with x-ray diffraction scans and phase diagram calculations in a way that extends the knowledge of these alloys for future research. The intent of this work is to demonstrate that the metal additive manufacturing technology, while impressive for fabricating complex net-shaped components, has the potential to change the paradigm for materials selection in mechanical design. By fabricating components with graded compositions, limitations in the properties of monolithic metal alloys can be circumvented, allowing access to hardware that was never before possible. We have shown that multi-component phase diagrams can be used as maps to transition from one desired material property to another and we have demonstrated that applying a rotational axis to the already net-shaped LD fabrication process can be used to generate alloys with radial composition gradients. Extending this work would involve the fabrication of many new gradient compositions and then identifying applications where the multifunctional properties of those gradients are most beneficial. Among the most highly desirable gradients are those from Ti-alloys to Al-alloys, from steel to Al-alloys and from Ti-alloys to steel.

Experimental Methods

Tension tests were performed on an Instron load frame traveling at a strain rate of 10^{-4} . The carbon fiber panels were made from M55J prepreg where each face skin was 8 plies thick at 5 mils per ply. BTCy-1A resin was used to bond to 5056 Al honeycomb (1/8 inch cell size, 3.1 lbs/ft³). EA 9394 adhesive was used to bond the inserts into the panels. The Ti-6Al-4V to V gradient was fabricated using 325 mesh powder of Ti-6Al-4V and pure V using 195 layers, each 0.38 mm thick. The travel speed was 12.7 mm/s, the working height was 9.53 mm, the substrate thickness was 6.35 mm, the atmosphere was Ar, flowing at 4.4 lpm. The build time was 585 min. The radial gradient alloy was fabricated using an A286 substrate and 325 mesh powder of 304 L and Invar 36. The spot size of the laser was 1.41 mm and the working height was 9.53 mm. The atmosphere was Ar with <10 ppm oxygen flowing at 3 lpm. The total build time was 180 min. Linear and rotational velocity and deposition rates are listed in Table 2. Thermodynamic calculations were performed using Thermo-Calc version 5¹⁹. A 2012 NIMS assessment based on was used for the Cr-Fe-Ni system²⁵. The COST 507 light metal alloy database was used for the Al-Ti-V system²².

- Hopkinson, N., Hague, R. & Dickens, P. *Rapid manufacturing: an industrial revolution for a digital age*. (Wiley-Blackwell, Berlin, 2005).
- Hague, R. J. M., Campbell, R. I. & Dickens, P. M. Implications on design of rapid manufacturing. *Proc. Inst. Mech. Eng. Part C: J. Mech. Eng. Sci.* **217**, 25–30 (2003).
- Campbell, R. I., Hague, R. J. M., Sener, B. & Wormald, P. W. The potential for the bespoke industrial designer. *The Des. J.* **6**, 24–34 (2003).
- Gibson, I., Rosen, D. W. & Stucker, B. *Additive manufacturing technologies: rapid prototyping to direct digital manufacturing*. (Springer, London, 2010).
- Santos, E. C., Shiomi, M., Osakada, K. & Laoui, T. Rapid manufacturing of metal components by laser forming. *Int. J. Mach. Tools and Manuf.* **46**, 1459–1468 (2006).
- Griffith, M. L. *et al.* Understanding the Microstructure and Properties of Components Fabricated by Laser Engineered Net Shaping (LENS). *MRS Proc.* **625**, 9 (2011).
- Bever, M. B. & Duwez, P. F. Gradients in composite materials. *Mater. Sci. Eng.* **10**, 1–8 (1972).
- Shen, M. & Bever, M. B. Gradients in polymeric materials. *J. Mater. Sci.* **7**, 741–746 (1972).
- Miyamoto, Y., Kaysser, W. A., Rabin, B. H., Kawasaki, A. & Ford, R. G. *Processing and Fabrication*. (Springer, London, 1999).
- Crespo, A. & Vilar, R. Finite element analysis of the rapid manufacturing of Ti-6Al-4V parts by laser powder deposition. *Scripta Mater.* **63**, 140–143 (2010).

- Lütjering, G. Influence of processing on microstructure and mechanical properties of ($\alpha + \beta$) titanium alloys. *Mat. Sci. and Eng.: A* **243**, 32–45 (1998).
- Kelly, S. & Kampe, S. Microstructural evolution in laser-deposited multilayer Ti-6Al-4V builds: Part I. Microstructural characterization. *Met. and Mater. Trans. A* **35**, 1861–1867 (2004).
- Lu, Y., Tang, H. B., Fang, Y. L., Liu, D. & Wang, H. M. Microstructure evolution of sub-critical annealed laser deposited Ti-6Al-4V alloy. *Mater. & Design* **37**, 56–63 (2012).
- Murr, L. E. *et al.* Microstructure and mechanical behavior of Ti-6Al-4V produced by rapid-layer manufacturing, for biomedical applications. *J. of the Mech. Beh. of Biomed. Mater.* **2**, 20–32 (2009).
- Banerjee, R., Collins, P. C., Bhattacharyya, D., Banerjee, S. & Fraser, H. L. Microstructural evolution in laser deposited compositionally graded α/β titanium-vanadium alloys. *Acta Mater.* **51**, 3277–3292 (2003).
- Collins, P. C., Banerjee, R., Banerjee, S. & Fraser, H. L. Laser deposition of compositionally graded titanium-vanadium and titanium-molybdenum alloys. *Mater. Sci. and Eng.: A* **352**, 118–128 (2003).
- Tan, H., Zhang, F., Chen, J., Lin, X. & Huang, W. Microstructure evolution of laser solid forming of Ti-Al-V ternary system alloys from blended elemental powders. *Chinese Opt. Lett.* **9**, 051403–51406 (2011).
- Liu, Z.-K. First-Principles Calculations and CALPHAD Modeling of Thermodynamics. *J. of Phase Equil. and Diff.* **30**, 517–534 (2009).
- Andersson, J.-O., Helander, T., Höglund, L., Shi, P. & Sundman, B. Thermo-Calc & DICTRA, computational tools for materials science. *Calphad* **26**, 273–312 (2012).
- Cao, W. *et al.* PANDAT software with PanEngine, PanOptimizer and PanPrecipitation for multi-component phase diagram calculation and materials property simulation. *Calphad* **33**, 328–342 (2009).
- Schwendner, K. I., Banerjee, R., Collins, P. C., Brice, C. A. & Fraser, H. L. Direct laser deposition of alloys from elemental powder blends. *Scripta Materialia* **45**, 1123–1129 (2001).
- Ansara, I., Dinsdale, A. T. & Rand, M. H. COST 507 Definition of Thermochemical and Thermophysical Properties to Provide a Database for the Development of New Light Alloys: Thermochemical Database for Light Metal Alloys. *Office for Official Publications of the European Communities* (1998).
- Xue, L. & Islam, M. U. Free-form laser consolidation for producing metallurgically sound and functional components. *J. of Laser App.* **12**, 160 (2000).
- Ganesh, P. *et al.* Laser rapid manufacturing of bi-metallic tube with Stellite-21 and austenitic stainless steel. *Prasad Trans. of The Indian Inst. of Metals* **62**, 169–174 (2009).
- Miettinen, J. Thermodynamic reassessment of Fe-Cr-Ni system with emphasis on the iron-rich corner. *Calphad*. **23**, 231–248 (1999).

Acknowledgments

This research was carried out at the Jet Propulsion Laboratory, California Institute of Technology, under a contract with the National Aeronautics and Space Administration (NASA) and funded through the Office of the Chief Technologist. The authors acknowledge G. Agnes, C. Bradford, P. Gardner, C. Morandi, J. Mulder, P. Willis, and RPM for useful discussions. The authors cite no conflict of interest.

Author contributions

D.C.H. designed the research and wrote the manuscript, J.-P.B. performed the experiments and mechanical testing, S.R. performed the x-ray diffraction and mechanical testing, R.P.D. designed the research and edited the paper, J.K. contributed to the figures, J.S. performed nanoindentation, A.A.S. edited the paper, Z.-K.L. and R.O. performed the modeling.

Additional information

Supplementary information accompanies this paper at <http://www.nature.com/scientificreports>

Competing financial interests: The authors declare no competing financial interests.

How to cite this article: Hofmann, D.C. *et al.* Developing Gradient Metal Alloys through Radial Deposition Additive Manufacturing. *Sci. Rep.* **4**, 5357; DOI:10.1038/srep05357 (2014).



This work is licensed under a Creative Commons Attribution-NonCommercial-NoDerivs 4.0 International License. The images or other third party material in this article are included in the article's Creative Commons license, unless indicated otherwise in the credit line; if the material is not included under the Creative Commons license, users will need to obtain permission from the license holder in order to reproduce the material. To view a copy of this license, visit <http://creativecommons.org/licenses/by-nc-nd/4.0/>